# Copolymers of Fluorene and Thiophene with Conjugated Side Chain for Polymer Solar Cells: Effect of Pendant Acceptors

HAIJUN FAN,[1,2] ZHIGUO ZHANG,[1] YONGFANG LI,[1] XIAOWEI ZHAN[1]

[1]Beijing National Laboratory for Molecular Sciences, CAS Key Laboratory of Organic Solids, Institute of Chemistry, Chinese Academy of Sciences, Beijing 100190, People's Republic of China

[2]Chinese Academy of Sciences, Graduate University, Beijing 100049, People's Republic of China

Received 15 November 2010; accepted 4 January 2011
DOI: 10.1002/pola.24568
Published online 24 January 2011 in Wiley Online Library (wileyonlinelibrary.com).

**ABSTRACT**: Two copolymers of fluorene and thiophene with conjugated side-chain pending acceptor end group of cyanoacetate (**P2**) and malononitrile (**P3**) were synthesized. Both polymers exhibit good thermal stability and low highest occupied molecular orbital level (−5.5 eV). In comparison with **P2**, **P3** exhibits stronger UV–vis absorption and higher hole mobility. Polymer solar cells based on **P3**:$PC_{71}BM$ exhibits a power conversion efficiency of 1.33% under AM 1.5, 100 mW/cm$^2$, which is three times of that based on **P2**:$PC_{71}BM$. The higher efficiency is attributed to better absorption, higher hole mobility, and the reduced phase separation scale in **P3**:$PC_{71}BM$ blend. The aggregate domain size in **P3**:$PC_{71}BM$ blend is 50 nm, much smaller than that in **P2**:$PC_{71}BM$ blend (200 nm). Tiny difference in the end groups on side chains of **P2** and **P3** leads to great difference in phase separation scale, charge transport, and efficiency of their photovoltaic devices. © 2011 Wiley Periodicals, Inc. J Polym Sci Part A: Polym Chem 49: 1462–1470, 2011

**KEYWORDS**: conjugated polymers; donor–acceptor; morphology; polyfluorenes; polymer solar cells; structure–property relations; synthesis

**INTRODUCTION** Recently, polymer solar cells (PSCs) have attracted much attention because of their unique advantages such as low cost, flexibility, light weight, and large-area device fabrication.[1–6] Intense interdisciplinary research in this field has led to a significant increase in their power conversion efficiency (PCE). Encouraging PCEs as high as 6–7% has been achieved from alternating copolymers based on 2,7-carbazole or benzo[1,2-*b*:4,5-*b*′]dithiophene.[7,8] Polyfluorenes exhibited good thermal and photochemical stability, low-lying highest occupied molecular orbital (HOMO) level, high mobility, and excellent blue-emitting properties.[9,10] However, their bandgaps are about 3.3 eV, which is too large to efficiently harvest sunlight. Incorporating an electron-donating (D) and/or -accepting (A) units into the main chain can lower bandgap and extend absorption of the polyfluorenes. PCEs as high as 4–5% have been achieved from alternating D-A copolymers based on fluorenes.[11–15] Thus, alternating D-A copolymers based on fluorene donor unit have been proven to be a promising class of p-type photoactive materials for application in PSCs.

A side-chain conjugation design strategy has been proposed based on the basic D-A concept, which combined the design of using conjugated side-chains pending electron-withdrawing end group as the acceptor components and conjugated backbones as the donor components.[16–24] In this architecture, side-chain end groups act not only as the main chromophores to extend the absorption and adjust the HOMO/LUMO energy levels because of intrachain charge transfer (ICT) with the backbone via conjugated bridges[16] but also as the functional groups to improve the miscibility with fullerene acceptors.[25] Thus, copolymers of fluorene,[16,20] silafluorene,[17] carbazole,[18,21,24] dithienopyrrole,[22] or phenothiazine[22] and triphenylamine with different pendant acceptor groups such as malononitrile and 1,3-diethyl-2-thiobarbituric acid were synthesized. PCEs as high as 2–4.7% have been achieved for the solar cells based on the blends of these polymers and fullerene derivative $PC_{71}BM$. The selection of end groups on side chains is of vital importance involving the D-A character and polarity of the end groups. However, research related to the effect of end groups on side chains remains rare.

Since introduction of the bulk heterojunction (BHJ) architecture in PSCs,[26] which comprise photoactive films with interpenetrating blends of electron-donor and electron-acceptor components for fast efficient exciton dissociation and enhanced charge transport, morphology of photoactive films has been regarded as a critical factor in determining the PCEs of the photovoltaic devices.[27–31] A key parameter judging the morphology to be good or bad is the phase separation state achieved, namely the scale of separated domains

Correspondence to: Y. F. Li (E-mail: liyf@iccas.ac.cn) or X. W. Zhan (E-mail: xwzhan@iccas.ac.cn)

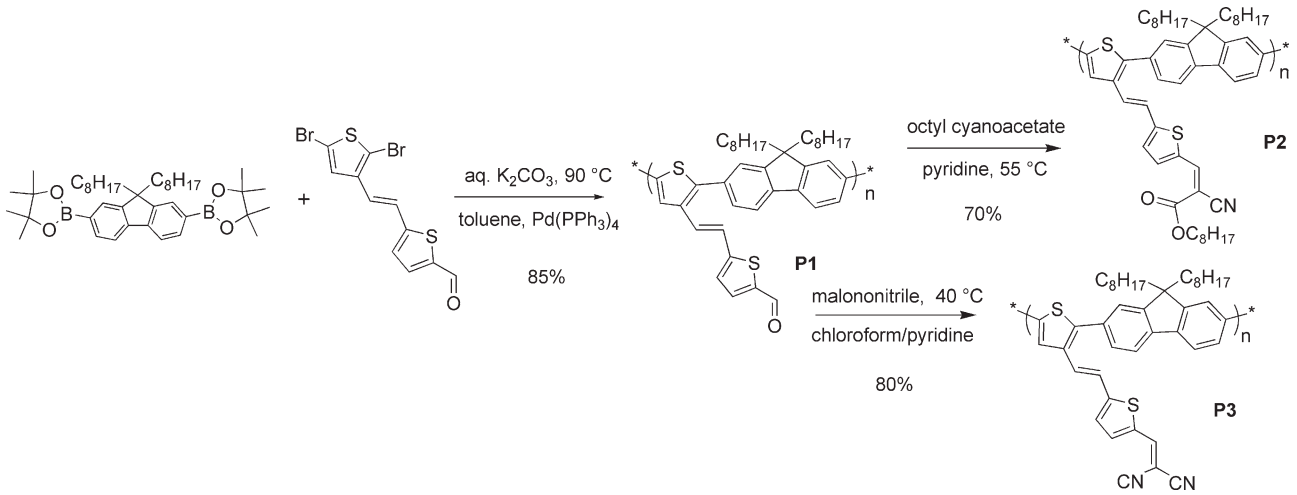


**SCHEME 1** Synthetic route of copolymers **P1**–**P3**.

in BHJ blend films.[32] In high-performance photovoltaic devices, an optimized intermediate scale of phase separation with direct percolation paths to the electrodes within each component of the blend, which maximizes charge separation while minimizing charge recombination, was demanded.[33] To achieve a proper phase separation, physical methods have been investigated, such as controlling the solvent evaporation rate by using mixture solvent or additive,[34,35] thermally annealing the photoactive layer after device fabrication,[36] and modifying the surface energy of the blend components and substrate.[37] Recently, methods by chemically modifying the chain structure of conjugated polymers through synthesis process have also been probed.[38,39] However, there has no report that performs both large phase separation transformation and significant PCE improvement of devices based on side-chain conjugated copolymers with pendant acceptors through a simple synthesis procedure.

In this work, we demonstrate synthesis and characterization of two conjugated copolymers of fluorene and thiophene with conjugated side-chain pending acceptor end groups of cyanoacetate (**P2**) and malononitrile (**P3**) (Scheme 1). Slight difference between **P2** and **P3** lies only on the end groups of side chains, whereas great difference on phase separation scale and PCE for their BHJ devices was observed. Devices based on **P3** exhibit two times enhancement of PCE because of much smaller phase separation scale relative to **P2**.

## EXPERIMENTAL

### Characterization

$^1$H NMR spectra were measured on a Bruker DMX-400 spectrometer. Chemical shifts were reported in ppm relative to the singlet of $CDCl_3$ at 7.26 ppm, and splitting patterns were designated as s (singlet), d (doublet), t (triplet), m (multiplet), and br (broaden). FTIR spectroscopy was performed on a Shimadzu FTIR-8400 spectrophotometer with KBr pellets. UV–visible absorption spectra were recorded by a UV-1601pc spectrometer. Number-($M_n$) and weight-average ($M_w$) molecular weights were measured by gel permeation chromatography (GPC) on a Waters GPC2410 with THF as an eluent and calibrated with polystyrene standards. Thermogravimetric analysis (TGA) was characterized by Perkin-Elmer Pyris 1 analyzer under a nitrogen atmosphere (100 mL/min) at a heating rate of 10 °C/min. Electrochemical cyclic voltammetry was conducted on a Zahner IM6e electrochemical workstation with Pt disk, Pt wire, and $Ag/Ag^+$ electrode (0.01 M $AgNO_3$, 0.09 M tetrabutylammonium hexafluorophosphate ($Bu_4NPF_6$) in acetonitrile) as working electrode, counter electrode, and reference electrode, respectively, in a 0.1 mol/L $Bu_4NPF_6$ acetonitrile solution.

### Fabrication and Characterization of PSCs

Patterned ITO glass (sheet resistance = 30 Ω/□) was precleaned first in an ultrasonic bath of acetone and isopropanol and treated in ultraviolet-ozone chamber (Jelight Company, USA) for 0.5 h. Then, a thin layer (30 nm) of poly(3,4-ethylenedioxythiophene):poly(styrene sulfonate) (PEDOT:PSS, Baytron P VP A1 4083, Germany) was spin coated onto the ITO glass and baked at 150 °C for 0.5 h. After that blend solution of **P2** (or **P3**) and $PC_{61}BM$ (or $PC_{71}BM$) in chloroform was spin coated onto the PEDOT:PSS film surface as the photoactive layers. Finally, an 80-nm aluminum layer was thermally evaporated onto the surface of the photosensitive layer under vacuum (ca. $10^{-5}$ Pa) through a shadow mask to form the cathode. The photoactive area of a single device was 4 $mm^2$, with a photoactive layer thickness of about 60 nm, measured by Ambios Technology XP-2 profilometer. The current density–voltage (*J*–*V*) characteristics were tested in glove box under simulated AM 1.5 G irradiation (100 mW/$cm^2$) with a computer-controlled Keithley 236 source measure unit using Oriel 96000 150 W solar simulator. The incident photon conversion efficiency (IPCE) was measured using a lock-in amplifier (SR830, Standford Research Systems) coupled with a WDG3 monochromator and a 500-W xenon lamp. The light intensity at each wavelength was calibrated with a calibrated silicon photovoltaic cell.

The nanoscale morphology of blend film was observed by an atomic force microscopy (AFM) (NanoMan VS, Veeco, USA) in

contact mode. Charge carrier mobility in blend films was measured by space charge limited current (SCLC) method.[40–42] The hole-only devices with the same active layer thickness as photovoltaic devices were fabricated with an ITO/PEDOT:PSS/photoactive layer/Au structure. The hole mobility was calculated by fitting the dark *J*–*V* curves for hole-only devices to SCLC model at low voltages, in which the current density is given by $J = 9\varepsilon_0\varepsilon_r\mu V^2/8L^3\exp[0.891\gamma(V/L)^{0.5}]$,[42] where $\varepsilon_0\varepsilon_r$ represents the permittivity of the material, $\mu$ the mobility, $\gamma$ the field activation factor, and $L$ is the thickness of the active layer. The applied bias voltage is corrected for the built-in potential so that $V = V_{applied} - V_{bi}$.

### Synthesis of Copolymer P1

2,7-Bis(4,4,5,5-tetramethyl-1,3,2-dioxaborolan-2-yl)-9,9-dioctylfluorene (643 mg, 1 mmol), 5-(2-(2,5-dibromothiophen-3-yl)vinyl)thiophene-2-carbaldehyde (378 mg, 1 mmol), $C_{25}H_{54}NCl$ (Aliquat 336, 20 mg), $Pd(PPh_3)_4$ (34 mg, 0.03 mmol), and toluene (6 mL) were charged into a 25-mL two-necked round-bottomed flask. A 2 M aqueous solution of $K_2CO_3$ (4 mL) was added. The mixture was deoxygenated with argon and stirred vigorously under argon at 90 °C for 48 h. The resulting mixture was then poured into 250 mL of methanol. The precipitate was collected after filtration and washed with 2 M HCl and methanol. The yellowish solid product of **P1** was Soxhlet extracted with acetone for 24 h to remove low-molecular-weight oligomers and catalyst residues (517 mg, 85%).

$^1$H NMR (400 MHz, $CDCl_3$): $\delta$ 9.85 (s, 1H), 7.88–7.77 (m, 2H), 7.71–7.67 (m, 4H), 7.59–7.52 (m, 2H), 7.38–7.30 (m, 2H), 7.18–7.17 (s, 1H), 2.10–2.07 (br, 4H), 1.26–1.12 (br, 24H), 0.80–0.78 (m, 6H). $M_n$, 41,841, $M_w/M_n$, 3.52.

### Synthesis of Copolymer P2

Octyl cyanoacetate (591 mg, 3 mmol) was added to a solution of **P1** (91.3 mg, 0.15 mmol of repeat unit) in 20 mL of pyridine. The solution turned red immediately and was stirred at 55 °C for 48 h. The solution was concentrated under reduced pressure. Polymer **P2** was precipitated by addition of methanol (150 mL) as a red solid (82 mg, 70%).

$^1$H NMR (400 MHz, $CDCl_3$): $\delta$ 8.22 (s, 1H), 7.91–7.74 (m, 6H), 7.59–7.52 (m, 2H), 7.43–7.28 (m, 2H), 7.20–7.17 (s, 1H), 4.44 (m, 2H), 2.11–2.18 (br, 4H), 1.75–1.66 (m, 2H), 1.26–1.11 (m, 34H), 0.80–0.79 (m, 9H). $M_n$, 59,158, $M_w/M_n$, 3.48.

### Synthesis of Copolymer P3

Malononitrile (198 mg, 3 mmol) was added to a solution of **P1** (91.3 mg, 0.15 mmol of repeat unit) in a mixture of chloroform (20 mL) and pyridine (1 mL). The solution color turned purple immediately and was stirred at 40 °C for 24 h. The solution was concentrated under reduced pressure. Polymer **P3** was precipitated by addition of methanol (150 mL) as a purple solid (78 mg, 80%).

$^1$H NMR (400 MHz, $CDCl_3$): $\delta$ 7.88–7.67 (m, 7H), 7.62–7.50 (m, 2H), 7.36–7.28 (m, 1H), 7.18–7.07 (m, 2H), 2.10–2.07 (br, 4H), 1.26–1.12 (br, 24H), 0.80–0.78 (m, 6H). $M_n$, 48,330, $M_w/M_n$, 3.36.

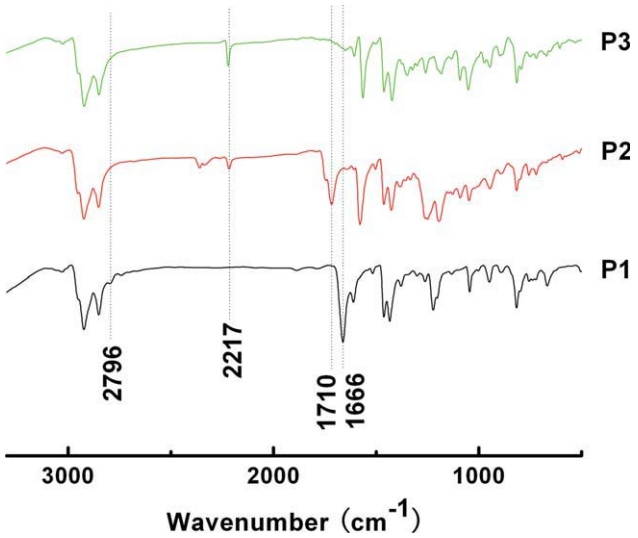


**FIGURE 1** FTIR spectra of the polymers (KBr pellets). [Color figure can be viewed in the online issue, which is available at wileyonlinelibrary.com.]

## RESULTS AND DISCUSSION

### Polymer Synthesis and Characterization

As shown in Scheme 1, the intermediate polymer **P1** was first synthesized via Suzuki coupling reaction in a yield of 85%. Then, the target polymers **P2** and **P3** were synthesized via reaction of the aldehyde end group on conjugated side chain with octyl cyanoacetate or malononitrile in yields of 70% (**P2**) and 80% (**P3**). As shown in FTIR spectra (Fig. 1), the characteristic peaks of CHO group in **P1** appear at 2796 and 1666 $cm^{-1}$, which is associated with the C—H and C=O stretching vibrations, respectively.[43] However, these two peaks disappear and new peaks emerge at 2217 (for **P2** and **P3**) and 1710 $cm^{-1}$ (for **P2** only), corresponding to the C≡N stretching vibration and the C=O stretching vibration, respectively.[20] In $^1$H NMR spectra, the aldehyde proton signal at 9.85 ppm disappears,[44] whereas olefinic proton signals at 8.22 for **P2** and 7.73 ppm for **P3** appear. These evidences support the efficient conversion of the aldehyde and the successful preparation of target polymers.

**P2** and **P3** exhibit good solubility in chloroform and THF. Molecular weights of the polymers were determined by GPC using polystyrene standards as calibrants (Table 1). **P2** and **P3** have weight-average molecular weight ($M_w$) of $2.0 \times 10^5$ and $1.6 \times 10^5$ with polydispersity index ($M_w/M_n$) of 3.48 and 3.36, respectively. The thermal properties of target polymers were investigated by TGA (Table 1). Both polymers **P2** and **P3** show good thermal stability with 5% weight loss occurring at 336 and 340 °C in nitrogen atmosphere.

### Optical Properties

The normalized UV–vis absorption spectra of the polymers in chloroform solution and films are shown in Figure 2. In solution [Fig. 2(a)], the maximum absorption peaks of **P2** and **P3**, corresponding to the $\pi$–$\pi^*$ transition of the polymer backbone, exhibit 10- to 15-nm red shift relative to that of

**TABLE 1** Molecular Weights, Yields, and Thermal Properties of **P2** and **P3**

| Polymer | $M_n$ | $M_w$ | $M_w/M_n$ | Yield (%) | $T_d$ (°C) |
|---|---|---|---|---|---|
| **P2** | 59,158 | 205,743 | 3.48 | 70 | 336 |
| **P3** | 48,330 | 162,390 | 3.36 | 80 | 340 |

**P1**. This could be attributed to the increased $\pi$-conjugation because of the introduction of the two kinds of side-chain end groups.[45] The new shoulder peaks at 486 (**P2**) and 500 nm (**P3**) indicate the intramolecular charge transfer (ICT) interactions between polymer backbone and side chain of **P2** and **P3**.[46] Stronger shoulder peak of **P3** indicates stronger withdrawing ability of dicyano end group and stronger ICT interaction compared to that in **P2**. In films of **P2** and **P3**, about 25-nm red shift of shoulder peaks were observed relative to that in solution [Fig. 2(b)], which are probably related to the formation of molecular aggregates and/or increased film polarization.[47,48]

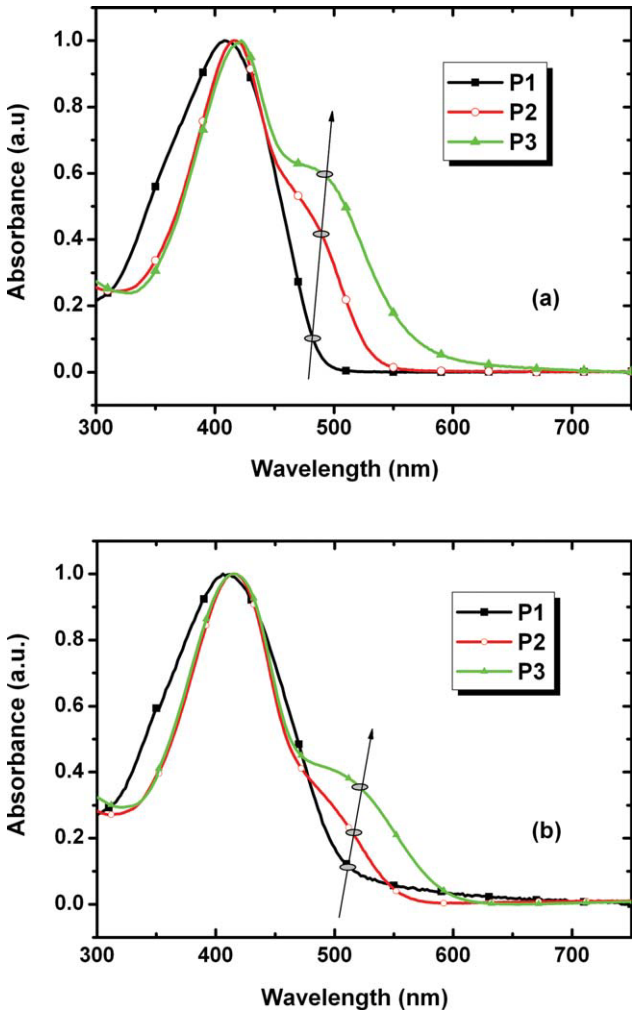


**FIGURE 2** UV–vis absorption spectra of the polymers in $CHCl_3$ solution (a) and in films (b). [Color figure can be viewed in the online issue, which is available at wileyonlinelibrary.com.]

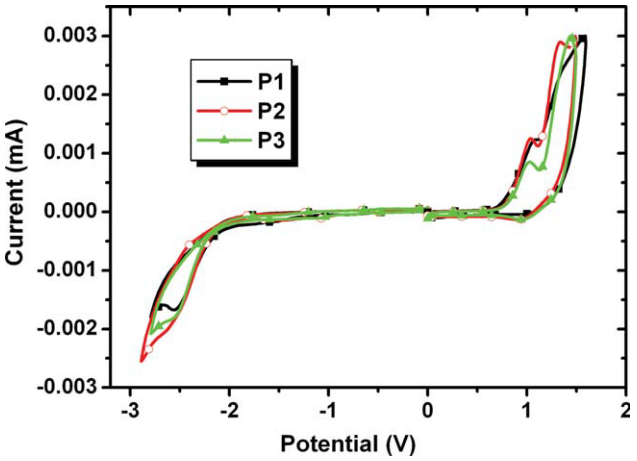


**FIGURE 3** Cyclic voltammograms for **P2** and **P3** in $CH_3CN$/0.1 M $[^nBu_4N]^+[PF_6]^-$ at 50 mV/s. The horizontal scale refers to $Ag/Ag^+$ reference electrode. [Color figure can be viewed in the online issue, which is available at wileyonlinelibrary.com.]

### Electrochemical Properties and Energy levels

Cyclic voltammograms of the polymers **P1**–**P3** are illustrated in Figure 3, and the onset oxidation and onset reduction potentials of the polymers are summarized in Table 2. All polymers displayed oxidation and reduction peaks. The HOMO energy levels of the polymers were calculated by $E_{HOMO} = -e(E_{ox} + 4.71)$ (eV), in which $E_{ox}$ represents the onset oxidation potential versus $Ag/Ag^+$. The lowest unoccupied molecular orbital (LUMO) energy levels were estimated by $E_{LUMO} = -e(E_{red} + 4.71)$ (eV), in which $E_{red}$ represents the onset reduction potential versus $Ag/Ag^+$. **P2** and **P3** exhibit a little lower HOMO and LUMO levels compared to **P1**. The energy level diagram for BHJ photovoltaic devices based on blend of **P2** or **P3** with $PC_{71}BM$ is also shown in Figure 4. The LUMO levels of **P2** and **P3** are higher than that of $PC_{71}BM$; the LUMO gaps between the donor and acceptor are large enough to guarantee photoinduced electron transfer between them. It is worth noting that the difference between the LUMO of acceptor and the HOMO of donor is as large as 1.6 eV (because of low HOMO of the donors **P2** and **P3**), which could lead to high open-circuit voltage ($V_{oc}$) of solar cells.

### Theoretical Calculations

To provide an intuitionistic insight into the molecular architecture of the polymers, molecular simulation was carried out for **P1**–**P3** with a chain length of $n = 2$ at the DFT B3LYP/6-31G (d) level with the Gaussian 03 program package.[49] The hexyl groups on the fluorene unit were not included for their unconspicuous effect on the equilibrium

**TABLE 2** Electrochemical Properties of Polymers **P1**–**P3**

| Polymer | $E_{ox}$ (V) | $E_{red}$ (V) | HOMO (eV) | LUMO (eV) |
|---|---|---|---|---|
| **P1** | 0.75 | −2.20 | −5.46 | −2.51 |
| **P2** | 0.80 | −2.18 | −5.51 | −2.53 |
| **P3** | 0.80 | −2.17 | −5.51 | −2.54 |

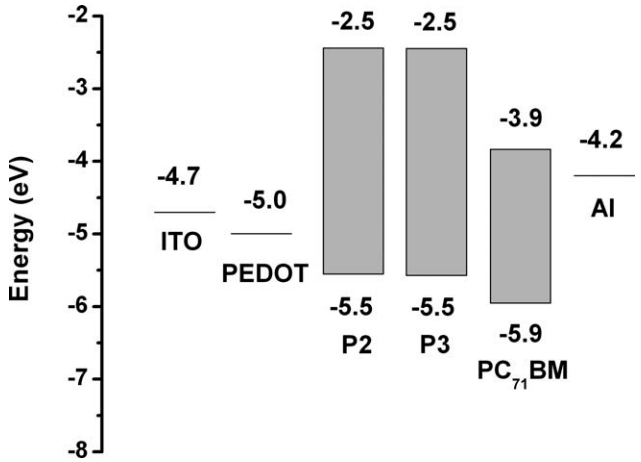


**FIGURE 4** Energy level diagram of BHJ photovoltaic devices.

geometry and electronic properties. Figure 5 gives the calculated molecular orbital geometry and energy levels. The LUMOs for all polymers are located on their side chains and adjacent thiophene rings, whereas the HOMOs are delocalized over both polymer backbones and side chains. The calculations show similar HOMO and lower LUMO levels for **P2** and **P3** relative to **P1**, which is in considerable coincidence with electrochemistry.

### Photovoltaic Properties

Photovoltaic properties of polymers **P2** and **P3** were investigated by fabricating BHJ photovoltaic devices, in which **P2** and **P3** were adopted as the donors to form the photoactive layers after blend with fullerene derivative acceptors. All devices follow the configuration of ITO/PEDOT:PSS/photoactive layer/Al. Improved performances have been made by optimizing the donor–acceptor ratios and the thicknesses of the active layers, selecting the suitable solvents, and adopting better acceptor material $PC_{71}BM$ with strengthened absorption. PSCs based on **P2** and **P3** give the best PCEs of 0.48 and 1.33%, respectively (Table 3, Fig. 6). The short-circuit current density ($J_{sc}$) seems to be the most responsible factor accounting for the difference between PCEs of devices based on **P2** and **P3**. The $J_{sc}$ of **P3**-based devices (4.33 mA/cm$^2$) is nearly three times of that of **P2** (1.45 mA/cm$^2$). The much higher $J_{sc}$ and PCE of **P3** was also confirmed by the IPCE measurement (Fig. 7). Device based on **P3** exhibits an IPCE peak of 52% at ~420 nm, which is three times of that based on **P2**.

**TABLE 3** Photovoltaic Properties of PSCs Based on **P2** and **P3**

| Active Layer | Ratio (w:w) | Thickness (nm) | $V_{oc}$ (V) | $J_{sc}$ (mA/cm$^2$) | FF | PCE (%) |
|---|---|---|---|---|---|---|
| **P2**:$PC_{71}BM$ | 1:1 | 90 | 0.80 | 1.45 | 0.41 | 0.48 |
| **P3**:$PC_{71}BM$ | 1:2 | 50 | 0.90 | 4.33 | 0.34 | 1.33 |

Different $J_{sc}$ generally involves three processes in BHJ solar cells, namely the generation of excitons, the diffusion of excitons to the D/A interfaces, and the transport of separated charges to the electrodes. The generation of exciton is closely related to the absorption of the active layers. With the same thickness (~60 nm), stronger absorption of **P3**:$PC_{71}BM$ blend film than **P2**:$PC_{71}BM$ blend film was observed (Fig. 8), confirming that the introduction of dicyano end groups on side chains of **P3** enhances the absorption of active layers and favors the generation of excitons.

The diffusion of excitons to the D/A interfaces and the transport of separated charges to the electrodes are intimately related to the phase separation state. Larger D/A interfaces, which facilitate the diffusion and separation of excitons, and

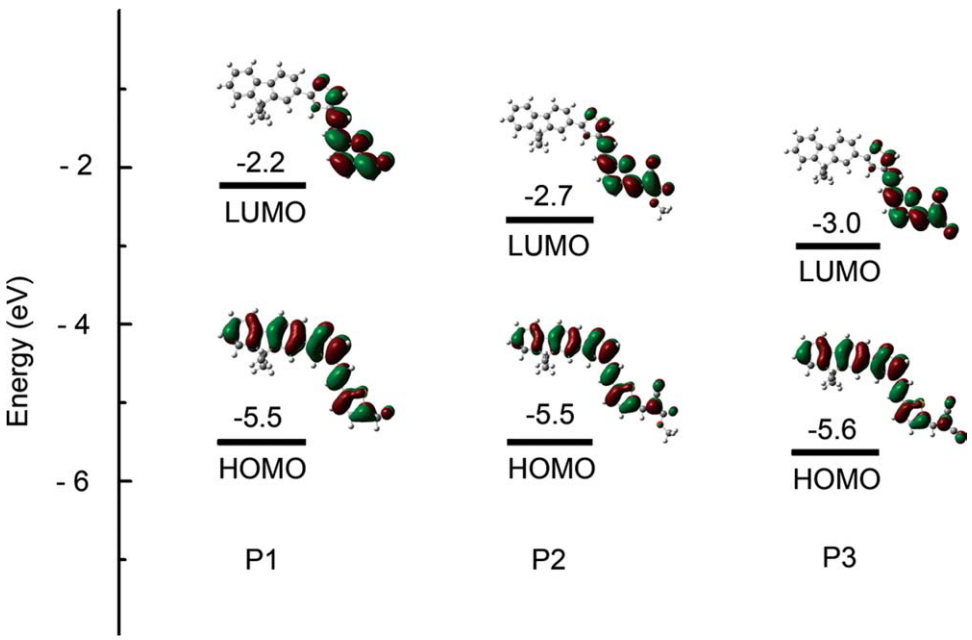


**FIGURE 5** Calculated molecular orbital geometry and energy levels obtained from DFT calculations on **P1**–**P3** with a chain length $n = 2$ at B3LYP/6-31G* level. [Color figure can be viewed in the online issue, which is available at wileyonlinelibrary.com.]

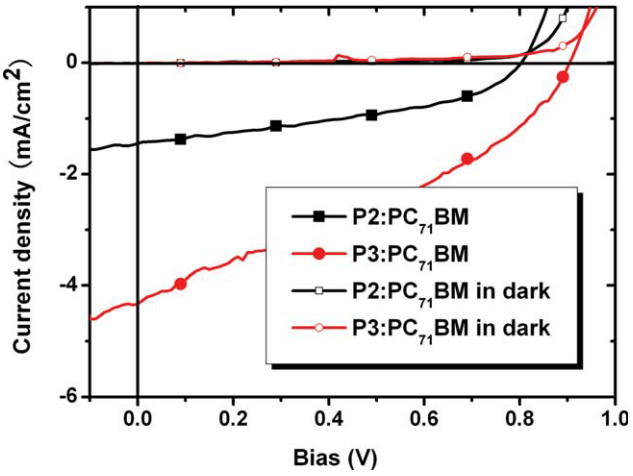


**FIGURE 6** Current density–voltage characteristics of PSCs based on **P2** and **P3**. [Color figure can be viewed in the online issue, which is available at wileyonlinelibrary.com.]

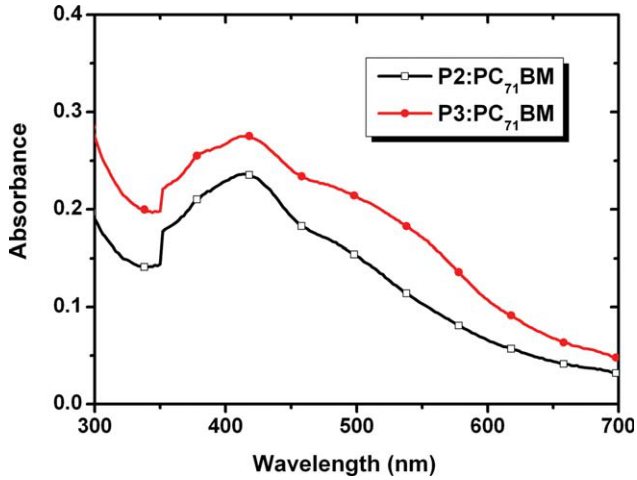


**FIGURE 8** UV–vis absorption spectra of **P2**:$PC_{71}BM$ and **P3**:$PC_{71}BM$ blend films. [Color figure can be viewed in the online issue, which is available at wileyonlinelibrary.com.]

faster charge transport, could be achieved by reducing the phase separation scale. An ideal nanoscale phase separation of less than 20 nm was recommended based on the consideration of the short exciton diffusion length of less than 10 nm in BHJ devices.[50,51] Figure 9 shows the actual phase separation state of blend films of **P2**:$PC_{71}BM$ and **P3**:$PC_{71}BM$. **P2**:$PC_{71}BM$ blend film gives coarser surface of a ~42-nm grain height and a 13.47-nm root-mean-square (RMS) roughness, whereas **P3**:$PC_{71}BM$ blend film gives much smaller phase separation with a ~1-nm grain height and a RMS roughness of 0.37 nm. From the cross-section profiles, domain size of **P2**:$PC_{71}BM$ blend film and **P3**:$PC_{71}BM$ blend is estimated to be about 200 and 50 nm, respectively; the latter seems much closer to the ideal phase separation scale.

To get further understanding, charge mobility in blend films was measured by SCLC method. On consideration of their difference, only hole mobility was characterized. Figure 10 shows the measured *J–V* curves for hole-only devices based on **P2** (or **P3**):$PC_{71}BM$ photoactive layers. The hole mobility ($\mu_h$) was calculated to be $2.12 \times 10^{-7}$ and $6.13 \times 10^{-7}$ $cm^2/V$ s for **P2** and **P3**, respectively. Polymer **P3** exhibits nearly three times of hole mobility of **P2** in the blend films, possibly because of the formation of more interpenetrating networks caused by the reduction of domain size.

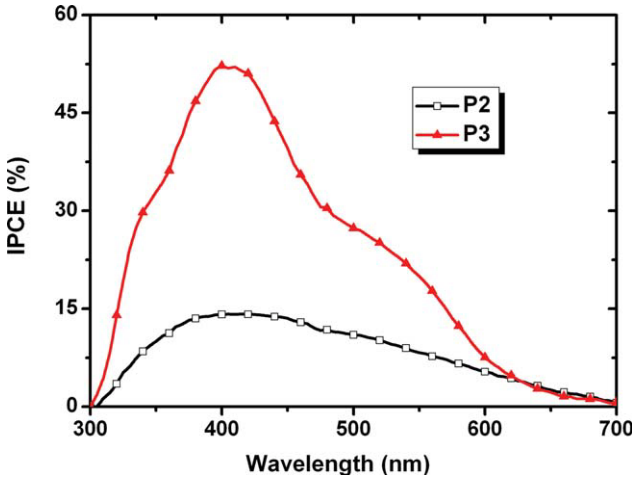


**FIGURE 7** IPCE curves of PSCs based on **P2** and **P3**. [Color figure can be viewed in the online issue, which is available at wileyonlinelibrary.com.]

Thus, based on comparison and analysis on absorption, morphology, mobility, and photovoltaic property of copolymers **P2** and **P3**, it can be inferred that the significant reduction in phase separation scale mainly leads to the big difference in device efficiency by increasing D/A interfaces, facilitating the diffusion and separation of excitons, and favoring the charge transport. The tiny structure difference in the end groups on side chains of **P2** and **P3** causes big difference in phase separation. Similarly, Andersson and coworkers reported that a reduced phase separation was caused by shortening or removing alkyloxy substituents.[52] Bo and coworkers reported that closely packing polymer main chain with smaller steric hindrance side chains helps to achieve higher performance.[53,54] Nguyen et al. found that in a poly(3-alkylthiophenes) (P3AT):$PC_{61}BM$ system, the longer side chains of P3AT enable the higher diffusion rate of $PC_{61}BM$ in the polymer matrix and ultimately lead to a larger scale phase separation.[55] Inspired by these examples, we suppose that the big difference in phase separation is related to the steric hindrance of side chain in **P2**. The longer carboxylic ester groups in **P2** are expected to favor the diffusion of $PC_{71}BM$, leading to a larger scale phase separation, disfavor the close packing of polymer main chain, and finally depress the efficiency.

## CONCLUSIONS

Two new conjugated copolymers of fluorene and thiophene with conjugated side-chain pending acceptor end group of

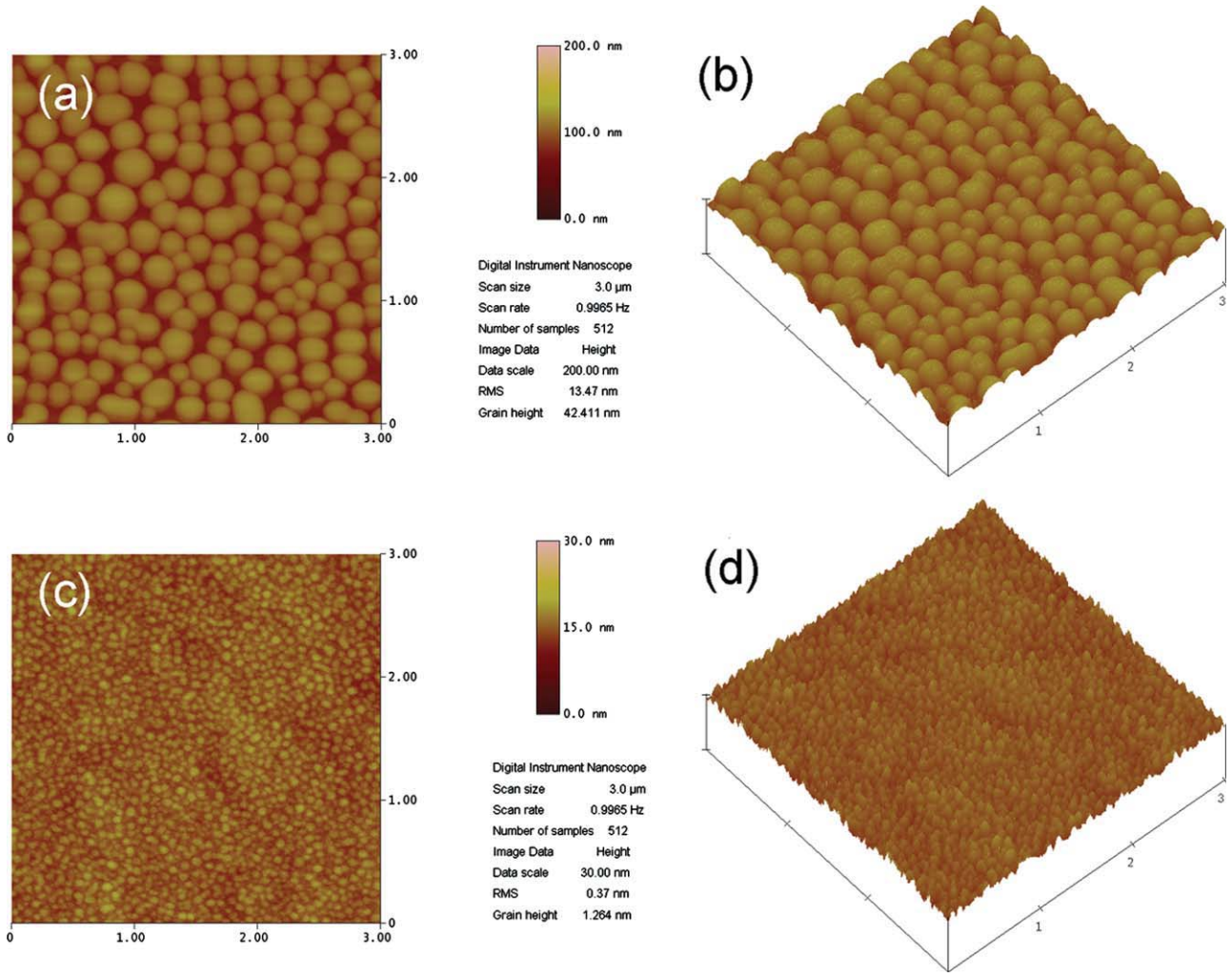


**FIGURE 9** AFM images of **P2**:$PC_{71}BM$ (a,b) and **P3**:$PC_{71}BM$ (c,d) blend films.

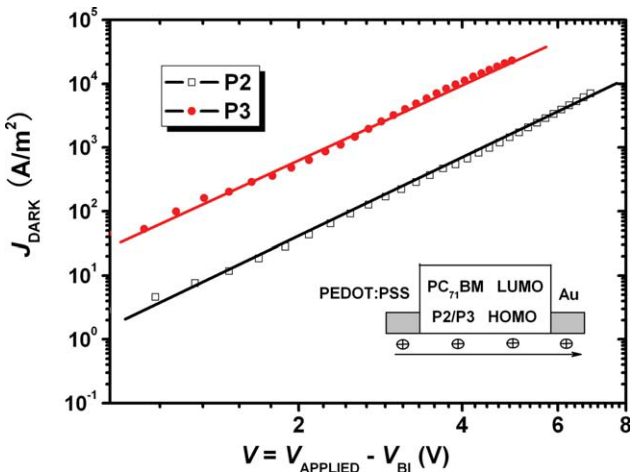


**FIGURE 10** Measured *J–V* characteristics under dark for determining the hole mobility of **P2** and **P3** using the single carrier device configuration. The solid lines represent the fit to the experimental data using SCLC model. The bias is corrected for built-in potential ($V_{bi}$), arising from difference in the work function of the contacts, so that $V = V_{applied} - V_{bi}$. $V_{bi}$ is 0.2 V for hole-only devices. [Color figure can be viewed in the online issue, which is available at wileyonlinelibrary.com.]

cyanoacetate (**P2**) and malononitrile (**P3**) were synthesized. Tiny difference in the end groups on side chains of **P2** and **P3** leads to great difference in phase separation scale, charge transport, and PCE for their BHJ devices. The longer carboxylic ester groups in **P2** favor the diffusion of $PC_{71}BM$, leading to a larger scale phase separation, and disfavor the close packing of polymer main chain, leading to a lower hole mobility. The significant reduction in phase separation scale of **P3**:$PC_{71}BM$ extends D/A interfaces, facilitates the diffusion and separation of excitons, and finally enhances the device efficiency. This work demonstrates an effective way to tune phase separation scale in PSCs by simple chemical modification.

Financial support by the NSFC (grants 21025418, 51011130028, 50633050, 21021091 and 20774104), 973 Project (grant 2011CB808401) and the Chinese Academy of Sciences is gratefully acknowledged.

## REFERENCES AND NOTES

**1** Arias, A. C.; MacKenzie, J. D.; McCulloch, I.; Rivnay, J.; Salleo, A. Chem Rev 2010, 110, 3–24.

**2** Gunes, S.; Neugebauer, H.; Sariciftci, N. S. Chem Rev 2007, 107, 1324–1338.

**3** Chen, J. W.; Cao, Y. Acc Chem Res 2009, 42, 1709–1718.

**4** Li, Y. F.; Zou, Y. P. Adv Mater 2008, 20, 2952–2958.

**5** Cheng, Y. J.; Yang, S. H.; Hsu, C. S. Chem Rev 2009, 109, 5868–5923.

**6** Zhan, X. W.; Zhu, D. B. Polym Chem 2010, 1, 409–419.

**7** Park, S. H.; Roy, A.; Beaupre, S.; Cho, S.; Coates, N.; Moon, J. S.; Moses, D.; Leclerc, M.; Lee, K.; Heeger, A. J. Nat Photon 2009, 3, 297–303.

**8** Chen, H. Y.; Hou, J. H.; Zhang, S. Q.; Liang, Y. Y.; Yang, G. W.; Yang, Y.; Yu, L. P.; Wu, Y.; Li, G. Nat Photon 2009, 3, 649–653.

**9** Abbel, R.; Schenning, A. P. H. J.; Meijer, E. J Polym Sci Part A: Polym Chem 2009, 47, 4215–4233.

**10** Zhan, X.; Liu, Y.; Wu, X.; Wang, S.; Zhu, D. Macromolecules 2002, 35, 2529–2537.

**11** Svensson, M.; Zhang, F. L.; Veenstra, S. C.; Verhees, W. J. H.; Hummelen, J. C.; Kroon, J. M.; Inganäs, O.; Andersson, M. R. Adv Mater 2003, 15, 988–991.

**12** Zhang, F.; Jespersen, K. G.; Bjorstrom, C.; Svensson, M.; Andersson, M. R.; Sundstrom, V.; Magnusson, K.; Moons, E.; Yartsev, A.; Inganäs, O. Adv Funct Mater 2006, 16, 667–674.

**13** Gadisa, A.; Mammo, W.; Andersson, L. M.; Admassie, S.; Zhang, F.; Andersson, M. R.; Inganäs, O. A. Adv Funct Mater 2007, 17, 3836–3842.

**14** Slooff, L. H.; Veenstra, S. C.; Kroon, J. M.; Moet, D. J. D.; Sweelssen, J.; Koetse, M. M. Appl Phys Lett 2007, 90, 143506.

**15** Kitazawa, D.; Watanabe, N.; Yamamoto, S.; Tsukamoto, J. Appl Phys Lett 2009, 95, 053701.

**16** Huang, F.; Chen, K. S.; Yip, H. L.; Hau, S. K.; Acton, O.; Zhang, Y.; Luo, J. D.; Jen, A. K. Y. J Am Chem Soc 2009, 131, 13886–13887.

**17** Duan, C. H.; Cai, W. Z.; Huang, F.; Zhang, J.; Wang, M.; Yang, T. B.; Zhong, C. M.; Gong, X.; Cao, Y. Macromolecules 2010, 43, 5262–5268.

**18** Duan, C. H.; Chen, K.-S.; Huang, F.; Yip, H.-L.; Liu, S.; Zhang, J.; Jen, A. K. Y.; Cao, Y. Chem Mater 2010, 22, 6444–6452.

**19** Hou, J. H.; Tan, Z. A.; Yan, Y.; He, Y. J.; Yang, C. H.; Li, Y. F. J Am Chem Soc 2006, 128, 4911–4916.

**20** Zhang, Z. G.; Zhang, K. L.; Liu, G.; Zhu, C. X.; Neoh, K. G.; Kang, E. T. Macromolecules 2009, 42, 3104–3111.

**21** Zhang, Z. G.; Liu, Y. L.; Yang, Y.; Hou, K. Y.; Peng, B.; Zhao, G. J.; Zhang, M. J.; Guo, X.; Kang, E. T.; Li, Y. F. Macromolecules 2010, 43, 9376–9383.

**22** Sahu, D.; Padhy, H.; Patra, D.; Huang, J.-H.; Chu, C.-W.; Lin, H.-C. J Polym Sci Part A: Polym Chem 2010, 48, 5812–5823.

**23** Wang, H. S.; Su, M. S.; Wei, K. H. J Polym Sci Part A: Polym Chem 2010, 48, 3331–3339.

**24** Hsu, S. L.; Chen, C. M.; Wei, K. H. J Polym Sci Part A: Polym Chem 2010, 48, 5126–5134.

**25** Gedefaw, D.; Zhou, Y.; Hellstrom, S.; Lindgren, L.; Andersson, L. M.; Zhang, F. L.; Mammo, W.; Inganäs, O.; Andersson, M. R. J Mater Chem 2009, 19, 5359–5363.

**26** Yu, G.; Gao, J.; Hummelen, J. C.; Wudl, F.; Heeger, A. J. Science 1995, 270, 1789–1791.

**27** Blom, P. W. M.; Mihailetchi, V. D.; Koster, L. J. A.; Markov, D. E. Adv Mater 2007, 19, 1551–1566.

**28** Thompson, B. C.; Fréchet, J. M. J. Angew Chem Int Ed Engl 2008, 47, 58–77.

**29** Dennler, G.; Scharber, M. C.; Brabec, C. J. Adv Mater 2009, 21, 1323–1338.

**30** Chen, L.-M.; Hong, Z.; Li, G.; Yang, Y. Adv Mater 2009, 21, 1434–1449.

**31** Yang, X.; Loos, J. Macromolecules 2007, 40, 1353–1362.

**32** McNeill, C. R.; Westenhoff, S.; Groves, C.; Friend, R. H.; Greenham, N. C. J Phys Chem C 2007, 111, 19153–19160.

**33** Shikler, R.; Chiesa, M.; Friend, R. H. Macromolecules 2006, 39, 5393–5399.

**34** Fan, H.; Shang, H.; Li, Y.; Zhan, X. Appl Phys Lett 2010, 97, 133302.

**35** Yao, Y.; Hou, J. H.; Xu, Z.; Li, G.; Yang, Y. Adv Funct Mater 2008, 18, 1783–1789.

**36** Ma, W. L.; Yang, C. Y.; Gong, X.; Lee, K.; Heeger, A. J. Adv Funct Mater 2005, 15, 1617–1622.

**37** Bjorstrom, C. M.; Nilsson, S.; Bernasik, A.; Budkowski, A.; Andersson, M.; Magnusson, K. O.; Moons, E. Appl Surf Sci 2007, 253, 3906–3912.

**38** Kim, J. S.; Lee, Y.; Lee, J. H.; Park, J. H.; Kim, J. K.; Cho, K. Adv Mater 2010, 22, 1355–1360.

**39** Hollinger, J.; Jahnke, A. A.; Coombs, N.; Seferos, D. S. J Am Chem Soc 2010, 132, 8546–8547.

**40** Murgatroyd, P. N. J Phys D: Appl Phys 1970, 3, 151–156.

**41** Shrotriya, V.; Yao, Y.; Li, G.; Yang, Y. Appl Phys Lett 2006, 89, 063505.

**42** Mihailetchi, V. D.; Xie, H. X.; Boer, B. D.; Koster, L. J. A.; Blom, P. W. M. Adv Funct Mater 2006, 16, 699–708.

**43** Fang, Q.; Yamamoto, T. Macromolecules 2004, 37, 5894–5899.

**44** Meng, F. S.; Liu, C. Z.; Hua, J. L.; Cao, Y.; Chen, K. C.; Tian, H. Eur Polym J 2003, 39, 1325–1331.

**45** Kim, J. S.; Lu, L.; Sreearunothai, P.; Seeley, A.; Yim, K. H.; Petrozza, A.; Murphy, C. E.; Beljonne, D.; Cornil, J.; Friend, R. H. J Am Chem Soc 2008, 130, 13120–13131.

**46** Leriche, P.; Frere, P.; Cravino, A.; Aleveque, O.; Roncali, J. J Org Chem 2007, 72, 8332–8336.

**47** Shang, Y. L.; Wen, Y. Q.; Li, S. L.; Du, S. X.; He, X. B.; Cai, L.; Li, Y. F.; Yang, L. M.; Gao, H. J.; Song, Y. J Am Chem Soc 2007, 129, 11674–11675.

**48** Surin, M.; Sonar, P.; Grimsdale, A. C.; Müllen, K.; Feyter, S. D.; Habuchi, S.; Sarzi, S.; Braeken, E.; Heyen, A. V.; Auweraer, M. V. D.; Schryver, F. C. D.; Cavallini, M.; Moulin, J. F.;

Biscarini, F.; Femoni, C.; Roberto, L.; Leclere, P. J Mater Chem 2007, 17, 728–735.

**49** Frisch, M. J.; Trucks, G. W.; Schlegel, H. B.; Scuseria, G. E.; Robb, M. A.; Cheeseman, J. R.; Montgomery, J. A., Jr.; Vreven, T.; Kudin, K. N.; Burant, J. C.; Millam, J. M.; Iyengar, S. S.; Tomasi, J.; Barone, V.; Mennucci, B.; Cossi, M.; Scalmani, G.; Rega, N.; Petersson, G. A.; Nakatsuji, H.; Hada, M.; Ehara, M.; Toyota, K.; Fukuda, R.; Hasegawa, J.; Ishida, M.; Nakajima, T.; Honda, Y.; Kitao, O.; Nakai, H.; Klene, M.; Li, X.; Knox, J. E.; Hratchian, H. P.; Cross, J. B.; Bakken, V.; Adamo, C.; Jaramillo, J.; Gomperts, R.; Stratmann, R. E.; Yazyev, O.; Austin, A. J.; Cammi, R.; Pomelli, C.; Ochterski, J. W.; Ayala, P. Y.; Morokuma, K.; Voth, G. A.; Salvador, P.; Dannenberg, J. J.; Zakrzewski, V. G.; Dapprich, S.; Daniels, A. D.; Strain, M. C.; Farkas, O.; Malick, D. K.; Rabuck, A. D.; Raghavachari, K.; Foresman, J. B.; Ortiz, J. V.; Cui, Q.; Baboul, A. G.; Clifford, S.; Cioslowski, J.; Stefanov, B. B.; Liu, G.; Liashenko, A.; Piskorz, P.; Komaromi, I.; Martin, R. L.; Fox, D. J.; Keith, T.; Al-Laham, M. A.; Peng, C. Y.; Nanayakkara, A.; Challacombe, M.; Gill, P. M. W.; Johnson, B.; Chen, W.; Wong, M. W.; Gonzalez, C.; Pople, J. A. Gaussian 03, Revision C. 02; Gaussian, Inc.: Wallingford, CT, 2004.

**50** Vacar, D.; Maniloff, E. S.; McBranch, D. W.; Heeger, A. J. Phys Rev B 1997, 56, 4573–4577.

**51** Shaw, P. E.; Ruseckas, A.; Samuel, I. D. W. Adv Mater 2008, 20, 3516–3520.

**52** Lindgren, L. J.; Zhang, F. L.; Andersson, M.; Barrau, S.; Hellstrom, S.; Mammo, W.; Perzon, E.; Inganäs, O.; Andersson, M. R. Chem Mater 2009, 21, 3491–3502.

**53** Li, W. W.; Qin, R. P.; Zhou, Y.; Andersson, M.; Li, F. H.; Zhang, C.; Li, B. S.; Liu, Z. P.; Bo, Z. S.; Zhang, F. L. Polymer 2010, 51, 3031–3038.

**54** Qin, R. P.; Li, W. W.; Li, C. H.; Du, C.; Veit, C.; Schleiermacher, H. F.; Andersson, M.; Bo, Z. S.; Liu, Z. P.; Inganäs, O.; Wuerfel, U.; Zhang, F. L. J Am Chem Soc 2009, 131, 14612–14613.

**55** Nguyen, L. H.; Hoppe, H.; Erb, T.; Gunes, S.; Gobsch, G.; Sariciftci, N. S. Adv Funct Mater 2007, 17, 1071–1078.